Research Square

Preprints are preliminary reports that have not undergone peer review.
They should not be considered conclusive, used to inform clinical practice,
or referenced by the media as validated information.

Evolution and Decay of Wind-Induced Rogue Waves: From Deep Ocean to Shallow Continental Shelves

Mirda Prisma Wijayanto
Universitas Jenderal Soedirman
Zulfa Siti Zakia
Universitas Jenderal Soedirman
Albertus Sulaiman
albe002@brin.go.id
Badan Riset dan Inovasi Nasionsl (BRIN), KST B.J. Habibie
Arief Darmawan
Badan Riset dan Inovasi Nasionsl (BRIN), KST B.J. Habibie
Jamrud Aminuddin
Universitas Jenderal Soedirman
Awaluddin Awaluddin
Badan Riset dan Inovasi Nasionsl (BRIN), KST B.J. Habibie
Asif Awaludin
Badan Riset dan Inovasi Nasionsl (BRIN), KST B.J. Habibie
Ginaldi A. Nugroho
Badan Riset dan Inovasi Nasionsl (BRIN), KST B.J. Habibie
Ibnu Fathrio
Badan Riset dan Inovasi Nasionsl (BRIN), KST B.J. Habibie

Research Article

Keywords: Benjamin-Feir Instability; Rogue Waves; FNLS, Mile's mechanism, Pulsation Effect, Uneven Bottoms

Posted Date: May 29th, 2026

DOI: https://doi.org/10.21203/rs.3.rs-9644835/v1

License: This work is licensed under a Creative Commons Attribution 4.0 International License.
Read Full License

Additional Declarations: No competing interests reported.

Evolution and Decay of Wind-Induced Rogue Waves: From Deep Ocean to Shallow Continental Shelves

Mirda Prisma Wijayanto[1)], Zulfa Siti Zakia[1)], Albertus Sulaiman[2)], Arief Darmawan[2)], Jamrud Aminuddin[1)], Awaluddin Awaluddin[2)], Asif Awaludin[2)], Ginaldi A. Nugroho[2)], Ibnu Fathrio[2)].

[1)]*Department of Physics, Faculty of Mathematics and Natural Sciences, Universitas Jenderal Soedirman Jl. Dr. Soeparno no. 61 Purwokerto, Indonesia, 53122*

[2)]*Research Center for Climate and Atmosphere, Badan Riset dan Inovasi Nasionsl (BRIN), KST B.J. Habibie, Serpong, Tangerang Selatan, Banten, Indonesia.*

Corresponding author: albertus sulaiman: albe002@brin.go.id

Abstract

Rogue waves are extreme waves that appear suddenly and can threaten ships and coastal structures. This study looks at how rogue waves form and change. They start in the open ocean when wind forces the water, then they move across the shallow continental shelf. The research focuses on a pulsation effect seen in field data, which suggests a rogue wave but does not prove the whole life cycle. In the open ocean, the growth of the waves is modeled with the Miles wind-input mechanism inside a forced nonlinear Schrödinger equation (forced NLSE). This approach captures both wind energy transfer and modulation instability in one framework. As the wave group reaches the continental shelf, a simple Boussinesq-type equation describes how the waves change due to finite depth and gentle bottom slopes. Using a WKB method, the study shows how the wave packet evolves with depth. Field observations confirm the rogue-wave signature after removing shoaling effects.

Keywords: *Benjamin-Feir Instability; Rogue Waves; FNLS, Mile's mechanism, Pulsation Effect, Uneven Bottoms.*

1. INTRODUCTION

Rogue waves, often referred to as freak waves and generally regarded as a special class of extreme wave events, are commonly identified as individual waves whose height substantially exceeds that of the surrounding sea state. These waves occur abruptly, persist for a relatively short duration, and may contain disproportionately large amounts of energy. Owing to these characteristics, they pose serious risks to ships, offshore platforms, and other marine infrastructure. Their prediction remains highly challenging because their occurrence is governed by a combination of nonlinear dynamics, random wave interference, wave–current interactions, and limited observational evidence. Linear wave theories and conventional statistical approaches are therefore often insufficient to describe their formation and evolution under realistic oceanic conditions (Kharif et al., 2009; Pelinovsky & Kharif, 2016).

The physical mechanisms responsible for rogue-wave formation are generally classified into two broad categories (Kharif and Toublout 2010, Pelinovsky and Kharif, 2016). The first comprises linear mechanisms, including dispersive focusing, geometrical focusing, and wave–current interactions. The second involves nonlinear mechanisms, particularly modulational instability, also known as Benjamin–Feir instability, which is associated with third-order nonlinear interactions in narrow-banded wave fields. These mechanisms have traditionally provided the theoretical basis for interpreting the emergence of extreme wave events in deep-water environments.

However, recent empirical and numerical studies have questioned the extent to which third-order nonlinear effects dominate rogue-wave formation under real oceanic conditions.

For example, Knobler et al. (2025) analyzed an 18-year dataset obtained from high-frequency laser altimeter measurements in the central North Sea, a region frequently exposed to severe sea states. Their findings suggest that rogue-wave occurrence is not necessarily governed primarily by higher-order nonlinear processes, such as Benjamin–Feir instability. Instead, they emphasize the importance of waveform asymmetry generated by second-order nonlinear effects, particularly through bound harmonics. Such asymmetry can enhance wave coupling and contribute to the amplification of extreme waves. Similar conclusions are also supported by analyses based on ERA5 reanalysis data and ECMWF CY47R1 wave-model hindcast products (Azevedo et al., 2025).

Wind forcing and shoaling have also been identified as important factors in understanding the development of rogue waves, particularly because these events may occur not only in the open ocean but also in coastal regions characterized by non-Gaussian sea states (Brunetti et al 2014, Ning et al., 2018; Wang et al., 2018; Jiang et al., 2020; Gemmrich and Cicon, 2022). In the open ocean, waves are often treated as deep-water waves, for which finite-depth effects are assumed to be negligible. By contrast, in finite-depth environments, rogue-wave dynamics are frequently described using models such as the Korteweg–de Vries equation, whereas the nonlinear Schrödinger equation is more appropriate for narrow-banded deep-water wave trains (Kharif and Pelinovsky, 2003). This distinction highlights the need for a framework that can account for the transition between wind-forced deep-water growth and finite-depth transformation over the continental shelf.

To address this gap, the present study examines the role of the wind drift layer in the formation and evolution of rogue-wave-like events. Although the wind drift layer may not act as a direct generating mechanism, it can significantly influence wave stability, focusing processes, and nonlinear wave interactions. Following Wagner et al. (2023), the wind drift layer is interpreted as a transitional region associated with changes from laminar to turbulent flow, within which wave focusing and second-order nonlinear interactions may be enhanced. This study therefore investigates how wind variability and wind-drift-layer dynamics affect the development of peak trough asymmetry and the focusing of second-order nonlinear energy. Specifically, the paper addresses the following research question: Does the presence of wind drift increase the likelihood of peak–trough asymmetry that promotes second-order nonlinear focusing in rogue-wave-like events?

2. THE METHODS

This study investigates the formation, transformation, and dissipation of extreme, rogue-wave-like wave groups that originate in the deep ocean and propagate toward the southern coast of Java. In the offshore region, wind forcing is represented through the Miles mechanism, which provides a pathway for energy transfer from the atmospheric boundary layer to the ocean surface. The resulting wave evolution is modeled using the forced nonlinear Schrödinger equation within the framework of Benjamin–Feir modulational instability (Maleewonf and Grimshaw 2022). As the wave group approaches the continental shelf, finite-depth effects, shoaling, and bathymetric variation become increasingly important in controlling its evolution. To describe this transition, a wave-packet approach is applied over gently varying slopes to

assess the persistence, modulation, and eventual decay of the extreme wave group. The model results are evaluated against field observations obtained from pressure-based wave-recording instruments deployed near the coast. The transition from deep-water to shallow-water wave dynamics is schematically illustrated in Figure 1.

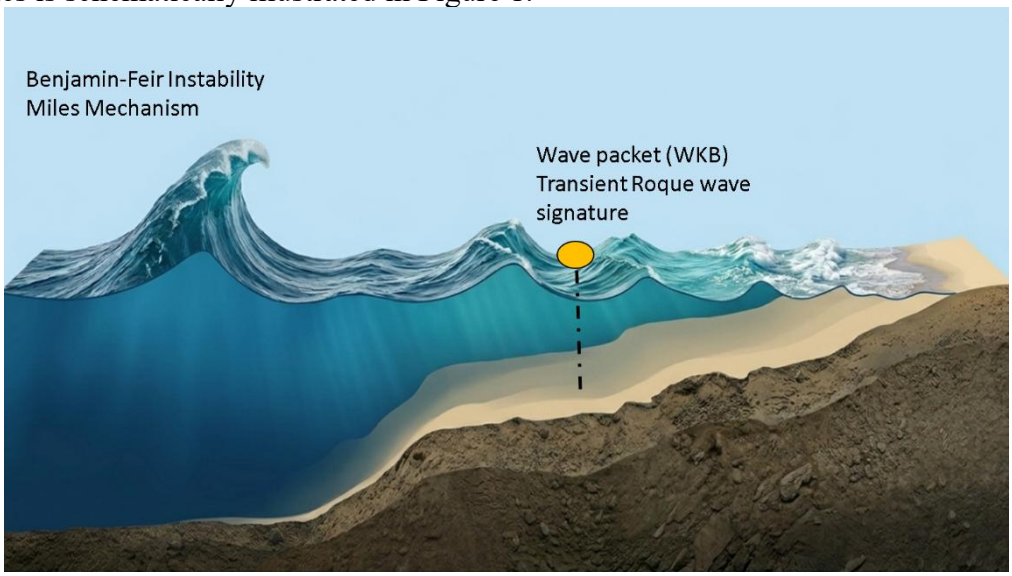

Figure 1. The schematic illustrates the complete life cycle of rogue waves, beginning with their genesis in the deep ocean and culminating in their impact on coastal regions. It maps the progression of physical domains deep-water and intermediate. Thus it explains how the waves move through different physical environments and the theories used in the research. Brown cycle represent a wave measurement.

2.1. The Model of Rogue Wave in the Deep Ocean: the forced and damped nonlinear Schrödinger equation

Benjamin and Feir (1967) demonstrated that uniform surface gravity waves in deep water are unstable to small sideband perturbations. Through nonlinear energy exchange between the carrier wave and its sidebands, initially weak disturbances may grow, producing a strongly modulated wave envelope and localized amplification of wave amplitude. This mechanism provides one of the theoretical foundations for understanding the emergence of rogue-wave-like events in narrow-banded wave fields. In the present study, wind-induced amplification in the drift layer is described using the forced nonlinear Schrödinger equation, following the formulation of Onorato and Proment (2012),

$$i\frac{\partial A}{\partial t}+\lambda\frac{\partial^2 A}{\partial x^2}+\mu|A|^2 A=i\Delta A, \tag{1}$$

where the water elevation is given by,

$$\eta(x,t)=\tfrac{1}{2}\left[A(x,t)e^{i(k_0x-\omega_0t)}+c.c.\right], \tag{2}$$

With the term of $exp(i(k_0x-\omega t))$ represent the fast propagate of carrier wave,

$$\mu = -\frac{\omega_o k_o^2}{4\sigma^2}(9\sigma^4 - 10\sigma^2 + 9) + \frac{g k_o \omega_o}{2\sigma^2(gh - c_g^2)}[2\sigma(3-\sigma^2) + 3k_0 h(1-\sigma^2)^2],$$

$$c_g = \frac{\partial \omega}{\partial k} = \frac{1}{2}\frac{\omega_o}{k_o}\left[1 + \frac{2k_o kh}{\sinh(2k_o h)}\right],\ \Delta = \frac{\rho_a \lambda \omega_0}{2g\rho_w k_0^2}\left(\frac{u_*}{c_g}\right)^2 - 2\nu k_0^2,\ \lambda = \frac{1}{2}\frac{d^2\omega}{dk^2},\ \text{and}\ \sigma = tanh(k_o h),$$

where A is the amplitude of slowly varying envelope, λ is the dispersion coefficient, ω_o is frequency, k_o is the wave number, h is the water depth, g is the gravitation acceleration, c_g is the group velocity, and Δ is the wind drift parameters. In this study we have derived an analytical solution to Equation (1) by taking into account the combined effects of dispersion, nonlinearity, and wind forcing. This solution lets us track the evolution of the wave envelope more accurately when the wind drift layer is present. Physically, the solution shows how the parameter Δ controls the growth rate of the modulation that leads to the formation of bright solitons these solitons are examples of extreme waves in a focusing system. We start with an ansatz,

$$A = Be^{\Delta t}, \qquad B(x,t) = \psi(\xi)e^{i(kx-\omega t)}, \quad \xi = x - vt, \tag{3}$$

Thus, we arrive (see Appendix –A),

$$A(x,t) = a_0 e^{2\Delta t}\,\mathrm{sech}\left[a_0 e^{\Delta t}(x - 2\lambda k t)\right]e^{i\left(kx - \lambda k^2 t + \frac{\lambda a_o^2}{2\Delta}e^{2\Delta t}\right)}. \tag{4}$$

When the external force Δ is vanish, we arrive

$$B_0(x,t) = a_0\,\mathrm{sech}\left[a_0(x - Vt)\right]e^{i\left(kx - \lambda k^2 t\right)}, \quad V = 2\lambda k. \tag{5}$$

The qualitative behavior of the nonlinear Schrödinger equation depends on the relative strength of the nonlinear and dispersive coefficients. This relationship may be expressed through the parameter $k=\mu/\lambda$, where the sign on k determines whether the system is focusing or defocusing. For $k > 0$, the system corresponds to the focusing regime and supports bright soliton-type solutions. For $k < 0$, the system is defocusing and may support dark solitons, which appear as localized amplitude depressions on a continuous wave background. Rogue-wave solutions arise in the focusing regime as a consequence of modulational instability, particularly Benjamin–Feir instability. Mathematically, the Peregrine soliton can be interpreted as a limiting form of the Akhmediev breather, which is periodic in space, or the Kuznetsov–Ma breather, which is periodic in time (Peregrine, 1983; Gaxiola and Biswas, 2018; Karjanto, 2021). Physically, such solutions describe a localized wave event whose amplitude may reach approximately three times the background amplitude and which is confined in both space and time. Under realistic oceanic conditions, persistent wind forcing and surface-current effects associated with the wind drift layer may enhance wave modulation and thereby increase the likelihood of transient extreme-wave amplification.

2.2.The Model of Rogue Wave in Shallow Continental Shelves: Low-Order Boussinesq Equations for Uneven Bottom

In the conceptual framework adopted here, extreme wave groups are assumed to form in offshore waters at depths greater than 500 m and more than 100 km from the observation point before propagating toward the 20 m coastal shelf. Because the characteristic water depth H is much smaller than the horizontal length scale L, and the wave amplitude A is much smaller than H, the nearshore propagation may be treated within the long-wave, weakly nonlinear regime. Accordingly, the transformation of the wave field over the continental shelf is described using a Boussinesq-type equation for weakly nonlinear, moderately long waves in shallow water (Mei et al., 2005),

$$\frac{\partial \eta}{\partial t}+\frac{\partial}{\partial x}\left[(h+\eta)u\right]=0, \tag{6}$$

$$\frac{\partial u}{\partial t}+u\frac{\partial u}{\partial x}+g\frac{\partial \eta}{\partial x}-\frac{h}{2}\frac{\partial^2}{\partial x^2}\left[h\frac{\partial u}{\partial t}\right]+\frac{h^2}{6}\frac{\partial^3 u}{\partial x^2\partial t}=0, \tag{7}$$

Derive Eq. (6) respect to t, assuming $\eta << h$, and linear shoaling, yields,

$$\frac{\partial \eta}{\partial t}+\frac{\partial (hu)}{\partial x}=0, \tag{8}$$

$$\frac{\partial u}{\partial t}+g\frac{\partial \eta}{\partial x}-\frac{h}{2}\frac{\partial^2}{\partial x^2}\left[h\frac{\partial u}{\partial t}\right]+\frac{h^2}{6}\frac{\partial^3 u}{\partial x^2\partial t}=0, \tag{9}$$

From Eq. (8), we obtaine $\frac{\partial (hu)}{\partial x}=-\frac{\partial \eta}{\partial t}$ and $\frac{\partial^2 (hu)}{\partial x^2}=-\frac{\partial^2 \eta}{\partial x\partial t}$ thus, we arrive,

$$\frac{\partial u}{\partial x}=-\frac{1}{h}\left(\frac{\partial \eta}{\partial t}+u\frac{\partial h}{\partial x}\right), \tag{10}$$

and,

$$h^2\frac{\partial^2 u}{\partial x^2}=-h\frac{\partial^2 \eta}{\partial x\partial t}+2\frac{\partial h}{\partial x}\frac{\partial \eta}{\partial t}+2\left(\frac{\partial h}{\partial x}\right)^2 u-h\frac{\partial^2 h}{\partial x^2}u\approx -h\frac{\partial^2 \eta}{\partial x\partial t}+2\frac{\partial h}{\partial x}\frac{\partial \eta}{\partial t}, \tag{11}$$

This is due to mild slope approximation. Thus, we obtaine a single equation for η (see Dingermans 1997 for detail derivation),

$$\frac{\partial^2 \eta}{\partial t^2}-\frac{\partial}{\partial x}\left(gh\frac{\partial \eta}{\partial x}\right)-\frac{1}{3}\frac{\partial^2}{\partial x\partial t}\left(h\frac{\partial h}{\partial x}\frac{\partial \eta}{\partial t}\right)=0. \tag{12}$$

For gently varying bathymetry, higher-order curvature terms and higher-order depth-gradient contributions may be neglected. Under this approximation, the governing system can be reduced to a single differential equation in terms of the surface elevation η. This reduction is useful because it permits either analytical treatment or efficient numerical solution while retaining the leading-order effects of weak nonlinearity, dispersion, and shoaling. However, this approximation is valid only when the bottom slope varies slowly over the characteristic

wavelength. If the bathymetric slope is steep or rapidly varying, the neglected higher-order terms may become significant and could affect the accuracy of the predicted wave evolution.

As a limiting case, we first consider constant depth, $h(x)=h_0$. By assuming a harmonic solution of the form $\eta \sim \exp(i(kx-\omega t))$, we obtain the following dispersion relation and the wave group velocity becomes,

$$\omega^2 = \frac{gh_0k^2}{\left[1+\frac{1}{3}h_0^2k^2\right]} \quad ; \quad v_g = \frac{\partial\omega}{\partial k} = \frac{\sqrt{gh_0}}{\left[1+\frac{1}{3}h_0^2k^2\right]^{\frac{3}{2}}}. \tag{13}$$

For a linearly varying depth, $h(x) = \alpha x$, the coefficients of the governing equation become spatially dependent. Consequently, the local wavelength changes as the wave propagates, reflecting the influence of shoaling. When the slope parameter α is sufficiently small, the bottom may be treated as locally uniform over one wavelength. This assumption allows a local dispersion relation and local group velocity to be defined at each position along the slope.

The transformation of the wave field is then modeled by solving Eq. (12) using a slowly varying wave-packet approximation (Yang, 2010). This approach enables the evolution of the wave envelope and its internal modulation structure to be tracked as the system transitions from the forced-NLS regime in deep water to the Boussinesq regime over the 20 m continental shelf. The approximation is formulated using a WKB-type method, in which the solution is represented as a rapidly oscillating carrier wave modulated by a slowly varying envelope in space and time. Introducing the slow variables X and T, together with the appropriate coordinate transformation,

$$X = \varepsilon x \quad , \quad T = \varepsilon t\,. \tag{14}$$

with ε is a small parameter. Substituting into Eq. (12) yields,

$$\varepsilon^2\left[\frac{\partial^2\eta}{\partial T^2} - \frac{\partial}{\partial X}\left(gh\frac{\partial\eta}{\partial X}\right)\right] - \frac{\varepsilon^4}{3}\frac{\partial^2}{\partial X\partial T}\left[h\left(\frac{\partial h}{\partial X}\right)\left(\frac{\partial\eta}{\partial T}\right)\right] = 0. \tag{15}$$

This framework provides a consistent basis for examining how initially amplified wave packets lose coherence and disperse as they propagate into shallower coastal waters. The WKB solution of the wave packet is expressed in terms of (Yang 1991),

$$\eta(x,t) \sim A(X,T)e^{i\Theta(X,T)/\varepsilon}, \tag{16}$$

where $\Theta(X,T)$ is the phase velocity, $A(X,T)$ is the amplitude that slowly varying function. Substituting Eq. (16) into Eq. (15), we get, the equation for amplitude

$$\frac{\partial^2 A}{\partial T^2} - g\frac{\partial h}{\partial X}\frac{\partial A}{\partial X} - gh\frac{\partial^2 A}{\partial X^2} = 0 \tag{17}$$

and for the phase,

$$A\frac{\partial^2\Theta}{\partial T^2} + \left(\frac{\partial A}{\partial X} + \frac{\partial A}{\partial T}\right)\frac{\partial\Theta}{\partial T} = 0 \tag{18}$$

2.3.Spectral Analysis and BFI Decomposition: Identifying Transient Rogue Wave Signatures

The observed free-surface elevation time series, $\eta(t)$, was analyzed using the fast Fourier transform to identify the dominant carrier frequency f_0 and its associated sideband pair $f_0 \pm \delta f$. These spectral components were isolated using band-pass filters in the frequency domain, after which an inverse Fourier transform was applied to reconstruct their temporal evolution. This procedure enables the energy exchange between the carrier and sidebands to be examined directly in the time domain and provides a diagnostic basis for identifying modulation instability. In Fourier-series terms, the reconstructed signal represents the superposition of the principal carrier frequency and its two dominant sidebands. The strength of the instability is quantified using the Benjamin–Feir Index, which compares the effect of nonlinear wave steepness with the stabilizing influence of spectral bandwidth. The BFI is expressed as

$$BFI-index=\frac{\varepsilon\sqrt{2}}{\delta/\omega_0}, \tag{19}$$

where ε denotes the characteristic wave steepness and δ represents the nondimensional spectral bandwidth. A higher *BFI-index* indicates a greater likelihood of instability and correlates with the rate at which energy grows in the decomposed sidebands, reflecting real physical conditions. When *BFI–index* > 1, the envelope $|A(t)|$ exhibits a pronounced modulation gain as the wave propagates.

The envelope of a time series can be studied with the Hilbert transform. A time series $\eta(t)$ is converted into a complex signal $Z(t) = \eta(t) + i\,H(\eta)$, where H is the Hilbert transform (Osborne 2010). A wave packet can be examined using a wave time series with the relation given by Osborne 2010.

$$|A(t)|=\sqrt{\eta^2(t)+\left(H\left[\eta(t)\right]\right)^2}. \tag{20}$$

This representation allows the wave packet to be analyzed in terms of its slowly varying amplitude modulation. Geometrically, the analytic signal rotates in the complex plane, and its distance from the origin at each time gives the instantaneous wave envelope. The resulting envelope traces the upper bound of the wave crests and provides a measure of the temporal evolution of wave-packet energy.

2.4.The Data

The field data used in this study represent background wind-generated wave conditions measured in the waters off Karang Potong, Saganten Village, Sindang Barang District, Cianjur Regency, West Java Province, Indonesia. The target deployment location of the wave-recording instrument was 7.481083° S and 107.165718° E, marked with an "X" in the corresponding site map, at an approximate water depth of 20 m. Wave measurements were collected continuously over a 24-hour period from 14 to 15 October 2024 using an SBE 26Plus instrument. This

instrument measures sea-level fluctuations using a pressure sensor, with a sampling interval of 0.25 s. The experimental configuration and deployment setting are shown in Figure 2.

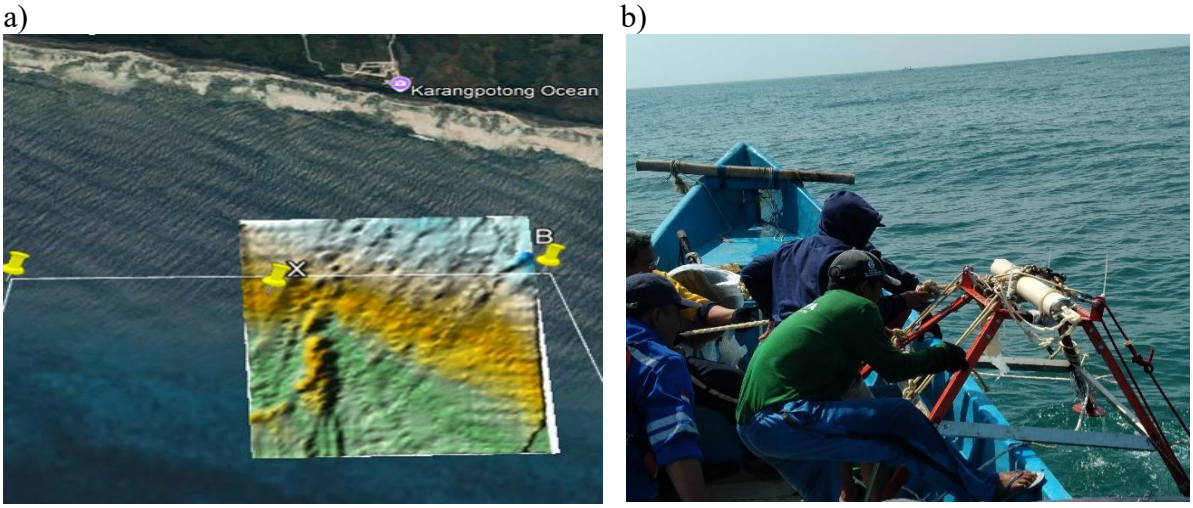

Figure 2. Wave observation scheme near the south coast of Java. a) The location of the wave measurement, b) wave instrument.

3. RESULT AND DISCUSSION

3.1.Generation and Propagation

The European Centre for Medium-Range Weather Forecasts (ECMWF) has issued a forecast indicating that strong winds will be present on 14 October 2024 (see Fig3a). This information is illustrated in Figure 3a, where wind speed exceeds 6.5 m s^{-1} over the affected region. Based on the simulation results, a wind speed of approximately 6.5 m s^{-1} places the environment in the Beaufort 4 (Moderate Breeze) category, which is a typical threshold for the onset of significant wave growth. The system's capacity to produce rogue waves hinges on the evolution of the amplitude term $A(x,t)$, which, according to the model, can increase three to four times its initial value as the wave packet propagates (Kharif and Pelinosky 2003). However, the mathematical formulation omits any dissipation or damping mechanisms, causing the amplitude to grow exponentially without bound. In reality, waves are constrained by a physical steepness limit: when the height-to-wavelength ratio surpasses the Stokes limit ($H/L \sim 1/7$ with H is the wave height and L is the wave length) (Babanin 2009), the wave becomes unstable and breaks, thereby limiting further amplification. Thus, the growth observed in the simulation represents an intense energy-pumping phase driven by the Miles mechanism, during which wind energy is transferred non-linearly into the wave field, producing extreme surges before the wave packet reaches its saturation point (see Fig.3b). The absence of a dissipation term means the model offers an upper bound on the energy that a wave packet could theoretically absorb, but it overestimates real-world outcomes because it neglects factors such as wave-wave interactions, turbulence, and bottom friction that would moderate the growth. Consequently, while the simulation highlights the potential for extreme wave formation under moderate wind conditions, it must be interpreted with caution, recognizing that actual oceanic waves will

experience energy losses that prevent the unbounded amplification predicted by the idealized model.

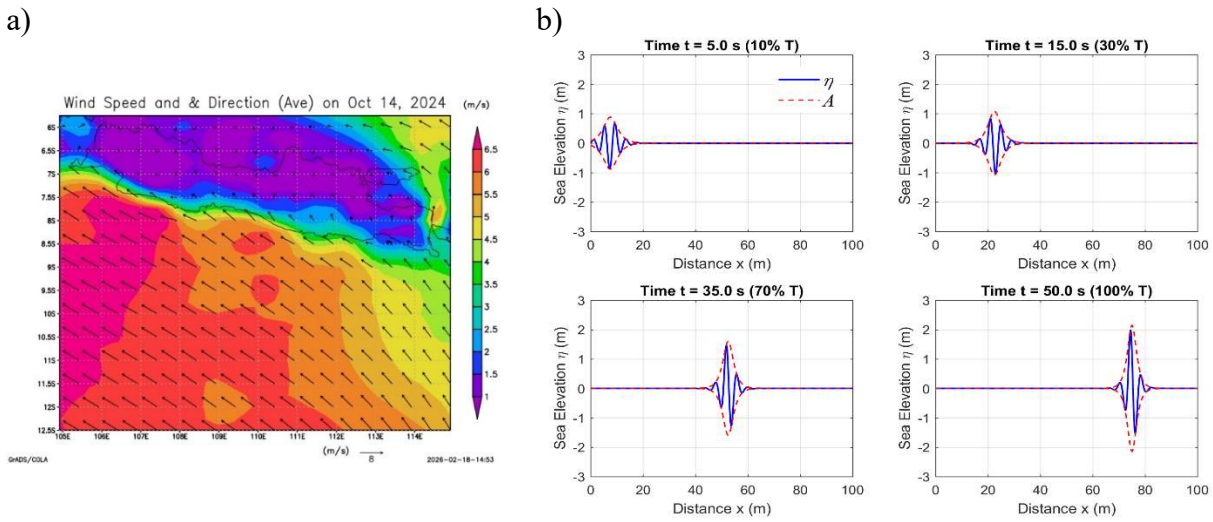

Figure 3. Extreme wave simulation using the Miles mechanism, a) Wind speed data from ECMWF for October 14, 2024, b) Wave evolution Eq. (1), simulation with a wind speed of 6.5 m/s.

Further, Figure 3 represent the existence of roque wave through Benjemin-Feir instability scheme. The scheme serves as a fundamental framework for understanding the emergence of rogue waves from initially linear wave phenomena, which become unstable due to nonlinear effects. Within the context of the Nonlinear Schrödinger Equation (NLS), the interplay between dispersion characterized by the dispersion relation and nonlinearity exemplified by amplitude-to-phase corrections and self-wave interactions facilitates modulational instability, commonly referred to as Benjamin–Feir instability (Hsiao and Maspero 2025). As the amplitude of the wave increases, the influence of nonlinear effects becomes increasingly significant, leading to a substantial growth of the wave envelope. This phenomenon is characterized by the transfer of energy from the carrier frequency to the modulation frequency, ultimately resulting in a marked increase in amplitude and the potential formation of rogue waves (Fedele et al 2016). This paper posits that such increases are particularly pronounced in the atmospheric wind drift layer, which exhibits heightened activity during extreme weather events.

3.2.Shallow Continental Shelves and existence of Roque waves

As the Roque wave moves toward the shoreline, it undergoes energy loss due to frictional dissipation and radiative effects. However, the variation in seabed depth bathymetry induces a shoaling process that amplifies the wave amplitude, making this effect significant for coastal impact assessments. To quantify the combined influence of dissipation and shoaling, we adopt the Wentzel–Kramers–Brillouin (WKB) method outlined in Eq. (16). This approach treats the wave as a slowly varying carrier whose envelope evolves according to the local depth profile, assuming a mild slope retaining the essential physics of wave-bottom interaction. The batimetry profile is expressed as,

$$h(x) = h_0 - H\left(\alpha + \beta erf\left[\frac{x-b}{a}\right]\right), \quad (21)$$

where h_0 is initial depth, H, α, β, a a b are constants, with $dh/dx_{max} << 1$ thus a mild slope approximation is fulfilled. This is depicted in Figure 4.

We commence by analyzing the characteristics of the surface wave that emerges from the background wave field, as inferred from 24-hour wave-gauge observations. To isolate the intrinsic variability of wind-driven waves, the tidal signal has been systematically removed. The temporal evolution of the wave envelope, extracted from these measurements, serves as a foundational baseline for the assessment of the onset and modulation of extreme wave events. We employed a demodulation technique using the Fourier Transform to analyze the three primary frequency components. The resultant wave spectrum is depicted in Figure 5. By examining the observational data, we extracted the amplitude and phase of each frequency (f_0 and its side frequencies) to reconstruct the sea surface elevation. This reconstruction enables us to observe the effects of the interaction between these harmonics on the temporal amplification of extreme waves. The results are illustrated in Figure 5. This result shows the pulsation effect, which arises when all three waves are perfectly in phase, leading to constructive interference. This alignment generates a single, towering peak referred to as a pulse (Longuet-Higgins, 1984). Shortly thereafter, the waves undergo destructive interference, causing them to cancel each other out and the ocean surface to appear calmer. The narrower the bandwidth of the waves, the longer the duration of the pulse. This means that the observed group of smaller waves gradually intensifies into a single massive wave, known as a Rogue Wave, before gradually receding. This process results in a distinct envelope profile (refer to Kharif & Touboul, 2010 for further clarification).

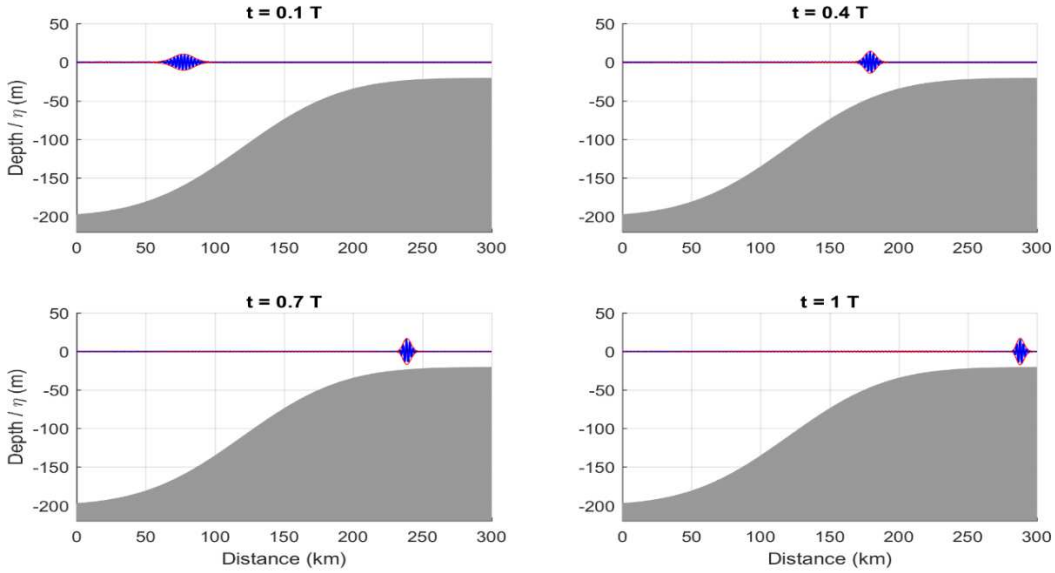

Figure 4. Simulation of Eq. (32) with mild slope approximation, with α is 50, β is 50, b is about 120 and a is 80. To avoid distorting the physics, we use Vertical Exaggeration (VE) when plotting: the calculation remains in the original scale (x-axis in km, y-axis in m), but the wave amplitude is drawn exaggerated so the bathymetry and wave profiles are clearly visible.

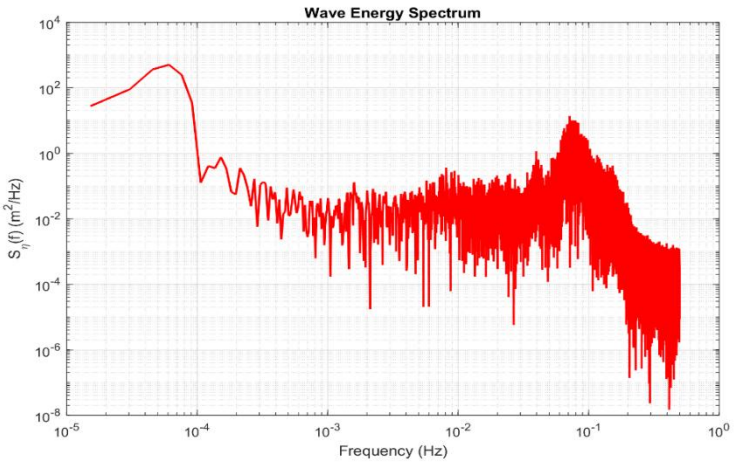

Figure 5. The wave spectrum of the wave generated by wind.

In this chapter we show how Roque waves appear on a coastal wave gauge. They are generated in the open sea by the Miles mechanism, shown in Figure 3. As the water depth changes, shoaling occurs; the wave-packet behaviour over gentle bathymetry is illustrated in Figure 4. First, we use a Hilbert transform to detect wave packets caused by shoaling. Next, we identify Roque waves using the BFI index: a single dominant frequency with two symmetric side peaks, as shown in Figure 5. It can be seen that the BFI index clearly highlights the presence of Roque waves. A spectrum profile with a single dominant frequency (f_0) flanked by two sidebands (δ) is a classic indication of a phenomenon known in hydrodynamics as modulation instability (Benjamin & Feir, 1967). This phenomenon generally indicates that a wave series that is initially uniform (carrier frequency f_0) tends to become unstable if its amplitude is large enough. This is because it is triggered by a small disturbance at a frequency very close to f_0. The side frequency δ is the frequency of this disturbance. Due to this energy transfer, the wave amplitude is no longer uniform, but instead forms 'pulses' or wave groups. At the peak of this modulation, the amplitude can increase drastically, reaching 2–3 times the average height, and behave nonlinearly (Wang et al. 2020). The frequency values above also indicate wind waves in shallow waters (in this case, 20 m). A bandwidth (δ) of 0.0008 Hz indicates a narrow band showing an unstable tendency (Wang et al. 2020; Janssen 2003; Berti et al. 2022). The envelope due to shoaling and the existence of rogue waves is depicted in Figure 6.

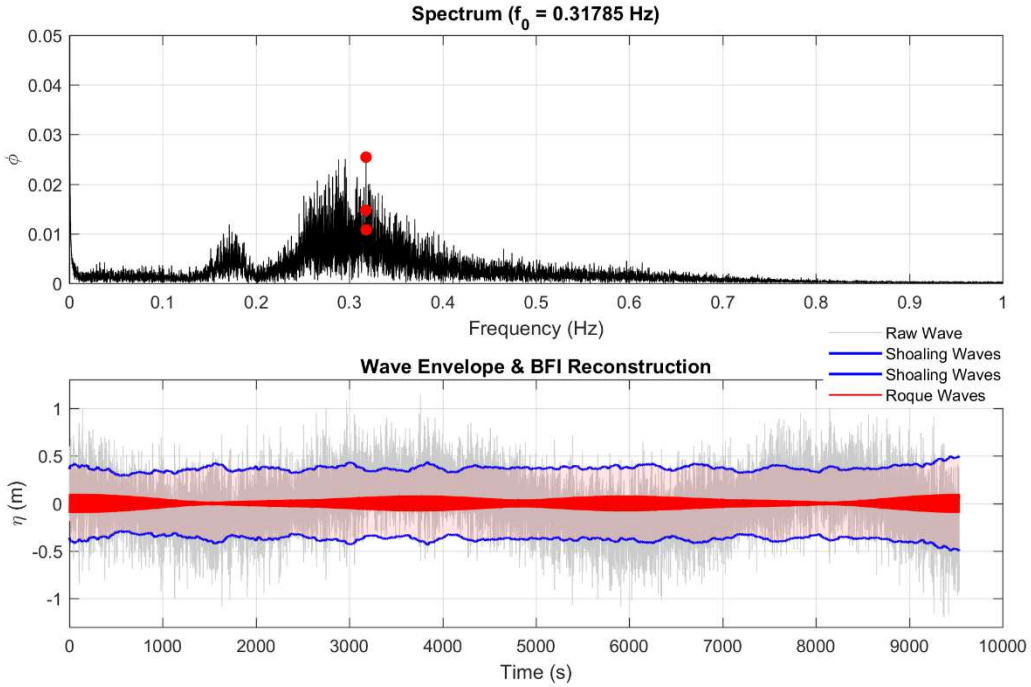

Figure 6. a) The Benjamin Feir Instability decomposition using Fourier analysis, with f_0 is 0.31785 Hz, and δ is about 0.0008 Hz, b) Envelope wave due to shoaling effect is represented in blue color, the signature Roque waves is depicted in red colour, and grey colour is wave data.

The figure 6, show that shoaling waves are the primary contributors to the observed wave spectrum, exhibiting a mean height of roughly one metre. This dominance arises because the water depth in the measurement area decreases, causing the waves to steepen and increase in amplitude as they approach the shoreline. In contrast, Roque waves characterized by a mean height of about 0.2 metres. The remaining wave energy, amounting to approximately 0.3 metres, can be attributed to wind-driven waves that propagate over a relatively uniform depth. These distinctions are critical when evaluating the BFI-index. The indexs is the ratio of wave steepness to spectral bandwidth, which serves as an indicator of the risk of extreme waves (Janssen 2003). A high BFI value would indicate a wave field dominated by a few coherent wave groups, whereas a low BFI suggests a more diffuse, wind-generated spectrum. However, some researchers argue that the BFI may underestimate the influence of shoaling effects in shallow water, proposing alternative metrics that incorporate depth-dependent wave transformations. With a wave number of 0.4066 rad/m, a slope of 0.0151, a bandwidth of 0.0008, and a relative depth of 8.131, we arrived at a BFI index of 12.9. This value signifies very unstable conditions and a heightened risk of extreme waves. The quotient of 2.98 indicates that the data are statistically normal, suggesting that this value is likely associated with either bandwidth or relative depth. Observational data show a water depth of 20 meters, which does not qualify as deep water. As such, the effects of shoaling are particularly pronounced (refer to May 1989 for a more detailed discussion). As waves approach the shore, shoaling amplifies their height, while dispersion concurrently occurs. The BFI index of 12.9 indicates that the increase in wave height resulting from shoaling happens much more rapidly than the dispersion

of wave energy. This situation leads to great instability in the waves prior to breaking. It is important to note that the BFI is inherently weaker in shallow waters, suggesting that the observed amplification is more likely due to shoaling rather than the BFI itself.

4. SUMMARY

This study investigates the life cycle of rogue waves, from their formation in deep water to their disappearance in shallow coastal areas. In the open ocean, wind energy drives the growth of wave groups through the Miles mechanism, which is described by the forced nonlinear Schrödinger equation (forced NLSE). Modulation instability, also known as the Benjamin–Feir instability, is the main cause of wave amplitude growth in deep water, and wind input greatly increases the growth of the wave envelope. As a wave packet moves toward the continental shelf, where the depth is about 20 m, it shifts from deep-water to shallow-water behavior. Using a WKB wave-packet approach, we show that this transition causes dispersive propagation and a gradual loss of phase coherence. Field observations at the coast consistently show pulsation effects, which we interpret as temporary amplification of wave groups. These observations confirm the presence of a rogue-wave signature; we used the WKB model to separate the effects of shoaling. Understanding this transition helps assess maritime hazards and protect coastal infrastructure. Overall, the study confirms that a wind drift layer increases the chance of crest-trough asymmetry, which drives nonlinear energy focusing. Although there is a decay in amplitude as they move towards shallow water, its signature can still be detected.

Acknowledgement

This worked support by Rumah Program ORKM 2025 and Rumah Program OREI 2025.

Contributor statement

MPW: analytical and numerical NLS equation, write paper, **ZSZ**: analytical analysis, **AS**: write a paper, wave packet and spectral analysis, **AD:** conceptualization, **JA**: Analysis and Interpretation, **AW:** Data curation, **AA**: data processing, **GAN**: field measurement, **IF**: Data quality.

External Funding:

We have no external funding

Clinical Number

In this research there are no Clinical Trial Number

Appendix A:
Analytical Solution of Eq. (1).

Eq. (1) describe a rogue wave genarated in the wind drift layer (Onorato and Proment 2012),

$$i\frac{\partial A}{\partial t}+\lambda\frac{\partial^2 A}{\partial x^2}+\mu\left|A\right|^2 A=i\Delta A, \tag{A1}$$

where the water elevation is given by,

$$\eta(x,t)=\tfrac{1}{2}\left[A(x,t)e^{i(k_0x-\omega_0t)}+c.c.\right], \tag{A2}$$

with the term of $\exp(\mathrm{i}(k_0x-\omega t))$ represent the fast propagate of carrier wave, and A is the amplitude of slowly varying envelope, λ is the dispersion coefficient, ω is frequency, k is the wave number, μ is the nonlinear coefficient, and Δ is the wind drift parameters. We propose a function that contains adjustable parameters. We substitute this function into the main equation and solve for the parameters so that the equation is satisfied. While choosing the function, we make sure that wind energy transfer remains physically continuous and that the wave envelope stays coherent (Osborne 2010). We start with an ansatz function,

$$A(x,t)=B(x,t)e^{\Lambda t}, \tag{A3}$$

Substituting into Eq.(A1), yields,

$$i\frac{\partial B}{\partial t}+\lambda\frac{\partial^2 B}{\partial x^2}+\mu e^{2\Delta t}\left|B\right|^2 B=0, \tag{A4}$$

This is time dependent of NLS equation. To solve it, we first study the solution structure for NLS with constant coefficients as follows.

$$i\frac{\partial B}{\partial t}+\lambda\frac{\partial^2 B}{\partial x^2}+\mu\left|B\right|^2 B=0, \tag{A5}$$

The solution in the traveling waves can be written as follow,

$$B(x,t)=\psi(\xi)e^{i(kx-\omega t)},\quad \xi=x-vt, \tag{A6}$$

Thus, the derivative become,

$$\frac{\partial B}{\partial t}=\left(-v\frac{\partial \psi}{\partial \xi}-i\omega\psi\right)e^{i(kx-\omega t)}, \tag{A7}$$

$$\frac{\partial B}{\partial x}=\left(\frac{\partial \psi}{\partial \xi}+ik\psi\right)e^{i(kx-\omega t)},\quad \frac{\partial^2 B}{\partial x^2}=\left(\frac{\partial^2 \psi}{\partial \xi^2}+2ik\frac{\partial \psi}{\partial \xi}-k^2\psi\right)e^{i(kx-\omega t)}. \tag{A8}$$

Subtituting into Eq. (5), yields,

$$\left[\lambda\frac{\partial^2\psi}{\partial\xi^2}+\mu\psi^3+\left(\omega-\lambda k^2\right)\psi\right]+i\left[\left(2\lambda k-v\right)\frac{\partial\psi}{\partial\xi}\right]=0. \tag{A9}$$

In the imaginary part we gave,

$$v=2\lambda k. \tag{A10}$$

Thus, in the real part, we have

$$\lambda\frac{\partial^2\psi}{\partial\xi^2}+\mu\psi^3+\left(\omega-\lambda k^2\right)\psi=0. \tag{A11}$$

Multiplying both side using $\partial\psi/\partial\xi$, we arrive,

$$\frac{\partial}{\partial\xi}\left(\frac{\partial\psi}{\partial\xi}\right)^2+\frac{\mu}{4\lambda}\frac{\partial\psi^4}{\partial\xi}-\frac{\left(\omega-\lambda k^2\right)}{2\lambda}\frac{\partial\psi^2}{\partial\xi}=0. \tag{A12}$$

Integrate this equation and set the integration constants are zero by invoking the vanishing boundary conditions at infinity, $\psi\rightarrow 0$ as $x\rightarrow\infty$, we arrive,

$$\left(\frac{\partial\psi}{\partial\xi}\right)^2=\frac{\left(\lambda k^2-\omega\right)}{\lambda}\psi^2-\frac{\mu}{2\lambda}\psi^4. \tag{A13}$$

Integration (integration constant set zero), we get the solution,

$$\psi(\xi)=\sqrt{\frac{2\left(\lambda k^2-\omega\right)}{\mu}}\,\mathrm{sech}\left(\sqrt{\frac{\left(\lambda k^2-\omega\right)}{\lambda}}\xi\right). \tag{A14}$$

Thus, we use an ansaltz, as follow,

$$B(x,t)=a(t)\,\mathrm{sech}\left(\xi(x,t)\right)e^{i\theta(x,t)},\quad \xi(x,t)=a(t)\left[x-x_0(t)\right],\quad \theta(x,t)=kx-\omega(t). \tag{A15}$$

The derivative opration becomes,

$$\frac{\partial B}{\partial t}=e^{i\theta}\left[\frac{\partial a}{\partial t}\,\mathrm{sech}\,\xi-a\,\mathrm{sech}\,\xi\tanh\xi\left(\frac{\partial a}{\partial t}\left(x-x_0\right)-a\frac{\partial x_0}{\partial t}\right)+ia\,\mathrm{sech}\,\xi\frac{\partial\theta}{\partial t}\right], \tag{A16}$$

$$\frac{\partial B}{\partial x}=e^{i\theta}\left[-a^2\,\mathrm{sech}\,\xi\tanh\xi+iak\,\mathrm{sech}\,\xi\right], \tag{A17}$$

$$\frac{\partial^2 B}{\partial x^2}=e^{i\theta}\left[-a^3\,\mathrm{sech}\,\xi\left(1-2\tanh^2\xi\right)-2ika^2\,\mathrm{sech}\,\xi\tanh\xi-k^2a\,\mathrm{sech}\,\xi\right], \tag{A18}$$

$$\left|B^2\right|B=a^3\,\mathrm{sech}^3\,\xi e^{i\theta} \tag{A19}$$

Substituting into Eq.(A4), we obtines,

$$\left[\lambda\left(-a^3\left(1-2\tanh^2\xi\right)-k^2a\right)-a\frac{\partial\theta}{\partial t}+\mu e^{2\Delta t}a^3\,\mathrm{sech}^3\,\xi\right]$$
$$+i\left[\frac{\partial a}{\partial t}-a\tanh\xi\left(\frac{\partial a}{\partial t}\left(x-x_0\right)-a\frac{\partial x_0}{\partial t}-2k\lambda a^2\tanh\xi\right)\right]. \tag{A20}$$

Again, the imaginary parth, we have

$$\tanh\xi=\frac{1}{a\left(x-x_0\right)}\quad,\quad x_0=2\lambda kt. \tag{A21}$$

and the real part, we obtain

$$\lambda=\frac{\mu a^2}{2a_0^2}\quad,\quad \omega(t)=\lambda k^2t-\frac{\lambda a_0^2}{2\Delta}e^{2\Delta t},\quad a=a_0e^{\Delta t}. \tag{A22}$$

Finally, we get the complete solution for *B(x,t)*,

$$B\left(x,t\right)=a_0e^{\Delta t}\,\mathrm{sech}\left[a_0e^{\Delta t}\left(x-2\lambda kt\right)\right]e^{i\left(kx-\lambda k^2t+\frac{\lambda a_o^2}{2\Delta}e^{2\Delta t}\right)}. \tag{A23}$$

Thus,

$$A\left(x,t\right)=a_0e^{2\Delta t}\,\mathrm{sech}\left[a_0e^{\Delta t}\left(x-2\lambda kt\right)\right]e^{i\left(kx-\lambda k^2t+\frac{\lambda a_o^2}{2\Delta}e^{2\Delta t}\right)}. \tag{A24}$$

Appendix B:
Derivation of WKB Approximation

The wave equation is given by,

$$\frac{\partial^2\eta}{\partial T^2}-\frac{\partial}{\partial X}\left(gh\frac{\partial\eta}{\partial X}\right)-\frac{\varepsilon^2}{3}\frac{\partial^2}{\partial X\partial T}\left[h\left(\frac{\partial h}{\partial X}\right)\left(\frac{\partial\eta}{\partial T}\right)\right]=0. \tag{B1}$$

Introduce a coordinate transform as follo,

$$X=\varepsilon x\quad,\quad T=\varepsilon t. \tag{B2}$$

We have deriavative operation

$$\frac{\partial}{\partial x}=\varepsilon\frac{\partial}{\partial X},\quad \frac{\partial}{\partial t}=\varepsilon\frac{\partial}{\partial T},\quad \frac{\partial^2}{\partial x^2}=\varepsilon^2\frac{\partial^2}{\partial X^2},\quad \frac{\partial^2}{\partial t^2}=\varepsilon^2\frac{\partial^2}{\partial T^2},\quad \frac{\partial^2}{\partial x\partial t}=\varepsilon^2\frac{\partial^2}{\partial X\partial T} \tag{B3}$$

Thus, (B1) becomes

$$\frac{\partial^2\eta}{\partial T^2}-\frac{\partial}{\partial X}\left(gh\frac{\partial\eta}{\partial X}\right)-\frac{\varepsilon^2}{3}\frac{\partial^2}{\partial X\partial T}\left[h\left(\frac{\partial h}{\partial X}\right)\left(\frac{\partial\eta}{\partial T}\right)\right]=0. \tag{B4}$$

We taje the WKB solution,

$$\eta(x,t) \sim A(X,T)e^{i\Theta(X,T)/\varepsilon}, \tag{B5}$$

Thus, the first term is,

$$\frac{\partial}{\partial T}\left(A(X,T)e^{i\frac{\Theta(X,T)}{\varepsilon}} \right) = \frac{\partial A}{\partial T}e^{i\frac{\Theta(X,T)}{\varepsilon}} + \frac{i}{\varepsilon}\frac{\partial \Theta}{\partial T}Ae^{i\frac{\Theta(X,T)}{\varepsilon}}$$

$$\frac{\partial^2 \eta}{\partial T^2} = \frac{\partial^2 A}{\partial T^2}e^{i\frac{\Theta(X,T)}{\varepsilon}} + \frac{i}{\varepsilon}\frac{\partial \Theta}{\partial T}\frac{\partial A}{\partial X}e^{i\frac{\Theta(X,T)}{\varepsilon}} + \frac{i}{\varepsilon}\frac{\partial^2 \Theta}{\partial T^2}Ae^{i\frac{\Theta(X,T)}{\varepsilon}} + \frac{i}{\varepsilon}\frac{\partial \Theta}{\partial T}\frac{\partial A}{\partial T}e^{i\frac{\Theta(X,T)}{\varepsilon}} - \frac{1}{\varepsilon^2}\left(\frac{\partial \Theta}{\partial T}\right)^2 Ae^{i\frac{\Theta(X,T)}{\varepsilon}} \tag{B6}$$

The second term,

$$\frac{\partial}{\partial X}\left(gh\frac{\partial \eta}{\partial X} \right) = \frac{\partial}{\partial X}\left(gh\left[\frac{\partial A}{\partial X}e^{i\frac{\Theta(X,T)}{\varepsilon}} + \frac{i}{\varepsilon}\frac{\partial \Theta}{\partial X}Ae^{i\frac{\Theta(X,T)}{\varepsilon}} \right] \right)$$

$$= g\frac{\partial h}{\partial X}\left[\frac{\partial A}{\partial X}e^{i\frac{\Theta(X,T)}{\varepsilon}} + \frac{i}{\varepsilon}\frac{\partial \Theta}{\partial X}Ae^{i\frac{\Theta(X,T)}{\varepsilon}} \right] + gh\frac{\partial}{\partial X}\left[\frac{\partial A}{\partial X}e^{i\frac{\Theta(X,T)}{\varepsilon}} + \frac{i}{\varepsilon}\frac{\partial \Theta}{\partial X}Ae^{i\frac{\Theta(X,T)}{\varepsilon}} \right]$$

$$= g\frac{\partial h}{\partial X}\left[\frac{\partial A}{\partial X}e^{i\frac{\Theta(X,T)}{\varepsilon}} + \frac{i}{\varepsilon}\frac{\partial \Theta}{\partial X}Ae^{i\frac{\Theta(X,T)}{\varepsilon}} \right] + gh\frac{\partial^2 A}{\partial X^2}e^{i\frac{\Theta(X,T)}{\varepsilon}} + \frac{i}{\varepsilon}gh\frac{\partial \Theta}{\partial X}\frac{\partial A}{\partial X}e^{i\frac{\Theta(X,T)}{\varepsilon}}$$

$$+ \frac{i}{\varepsilon}gh\frac{\partial^2 \Theta}{\partial X^2}Ae^{i\frac{\Theta(X,T)}{\varepsilon}} + \frac{i}{\varepsilon}gh\frac{\partial \Theta}{\partial X}\frac{\partial A}{\partial X}e^{i\frac{\Theta(X,T)}{\varepsilon}} + \frac{i}{\varepsilon}gh\left(\frac{\partial \Theta}{\partial X}\right)^2 Ae^{i\frac{\Theta(X,T)}{\varepsilon}} \tag{B7}$$

The third term,

$$\frac{\partial^2}{\partial X \partial T}\left[h\left(\frac{\partial h}{\partial X}\right)\left(\frac{\partial \eta}{\partial T}\right) \right] = \frac{\partial^2}{\partial X \partial T}\left[h\left(\frac{\partial h}{\partial X}\right)\frac{\partial A}{\partial T}e^{i\frac{\Theta(X,T)}{\varepsilon}} + \frac{i}{\varepsilon}h\left(\frac{\partial h}{\partial X}\right)\frac{\partial \Theta}{\partial T}Ae^{i\frac{\Theta(X,T)}{\varepsilon}} \right] =$$

$$\frac{\partial}{\partial X}\left[h\left(\frac{\partial h}{\partial X}\right)\left[\frac{\partial^2 A}{\partial T^2}e^{i\frac{\Theta(X,T)}{\varepsilon}} + \frac{i}{\varepsilon}h\left(\frac{\partial h}{\partial X}\right)Ae^{i\frac{\Theta(X,T)}{\varepsilon}} \right] + \frac{i}{\varepsilon}h\left(\frac{\partial h}{\partial X}\right)\left(\frac{\partial^2 \Theta}{\partial T^2}Ae^{i\frac{\Theta(X,T)}{\varepsilon}} + \frac{i}{\varepsilon}\left(\frac{\partial \Theta}{\partial T}\right)^2 \frac{\partial \Theta}{\partial T}Ae^{i\frac{\Theta(X,T)}{\varepsilon}} \right) \right] \tag{B8}$$

First term is

$$\frac{\partial}{\partial X}\left[h\left(\frac{\partial h}{\partial X}\right)\left(\frac{\partial^2 A}{\partial T^2}e^{i\frac{\Theta(X,T)}{\varepsilon}} + \frac{i}{\varepsilon}h\left(\frac{\partial h}{\partial X}\right)Ae^{i\frac{\Theta(X,T)}{\varepsilon}} \right) \right] = \left(\frac{\partial h}{\partial X}\right)^2 \left(\frac{\partial^2 A}{\partial T^2}e^{i\frac{\Theta(X,T)}{\varepsilon}} + \frac{i}{\varepsilon}h\left(\frac{\partial h}{\partial X}\right)Ae^{i\frac{\Theta(X,T)}{\varepsilon}} \right)$$

$$+ h\frac{\partial^2 h}{\partial X^2}\left(\frac{\partial^2 A}{\partial T^2}e^{i\frac{\Theta(X,T)}{\varepsilon}} + \frac{i}{\varepsilon}h\left(\frac{\partial h}{\partial X}\right)Ae^{i\frac{\Theta(X,T)}{\varepsilon}} \right) + h\left(\frac{\partial h}{\partial X}\right)\frac{\partial}{\partial X}\left(\frac{\partial^2 A}{\partial T^2}e^{i\frac{\Theta(X,T)}{\varepsilon}} + \frac{i}{\varepsilon}h\left(\frac{\partial h}{\partial X}\right)Ae^{i\frac{\Theta(X,T)}{\varepsilon}} \right) \tag{B9}$$

Due to mild slope (we ignore h^3 and the second derivative of h), we arrive,

$$\frac{\partial}{\partial X}\left[h\left(\frac{\partial h}{\partial X}\right)\left(\frac{\partial^2 A}{\partial T^2}e^{i\frac{\Theta(X,T)}{\varepsilon}}+\frac{i}{\varepsilon}h\left(\frac{\partial h}{\partial X}\right)Ae^{i\frac{\Theta(X,T)}{\varepsilon}}\right)\right]=\left(\frac{\partial h}{\partial X}\right)^2\frac{\partial^2 A}{\partial T^2}e^{i\frac{\Theta(X,T)}{\varepsilon}}+h\left(\frac{\partial h}{\partial X}\right)\frac{\partial^3 A}{\partial X\partial T^2}e^{i\frac{\Theta(X,T)}{\varepsilon}}$$
$$+\frac{i}{\varepsilon}h\left(\frac{\partial h}{\partial X}\right)\frac{\partial^2 A}{\partial T^2}\frac{\partial\Theta}{\partial X}e^{i\frac{\Theta(X,T)}{\varepsilon}} \tag{B10}$$

The seond term of right-handed side, yields

$$\frac{\partial}{\partial X}\left[\frac{i}{\varepsilon}h\left(\frac{\partial h}{\partial X}\right)\left(\frac{\partial^2\Theta}{\partial T^2}Ae^{i\frac{\Theta(X,T)}{\varepsilon}}+\frac{i}{\varepsilon}\left(\frac{\partial\Theta}{\partial T}\right)^2\frac{\partial\Theta}{\partial T}Ae^{i\frac{\Theta(X,T)}{\varepsilon}}\right)\right]=\frac{i}{\varepsilon}\left(\frac{\partial h}{\partial X}\right)^2\left(\frac{\partial^2\Theta}{\partial T^2}Ae^{i\frac{\Theta(X,T)}{\varepsilon}}+\frac{i}{\varepsilon}\left(\frac{\partial\Theta}{\partial T}\right)^2\frac{\partial\Theta}{\partial T}Ae^{i\frac{\Theta(X,T)}{\varepsilon}}\right)$$
$$+\frac{i}{\varepsilon}h\frac{\partial^2 h}{\partial X^2}\left(\frac{\partial^2\Theta}{\partial T^2}Ae^{i\frac{\Theta(X,T)}{\varepsilon}}+\frac{i}{\varepsilon}\left(\frac{\partial\Theta}{\partial T}\right)^2\frac{\partial\Theta}{\partial T}Ae^{i\frac{\Theta(X,T)}{\varepsilon}}\right) \tag{B11}$$

Due to mild slope (we ignore h^3 and the second derivative of h), we arrive,

$$\frac{\partial}{\partial X}\left[\frac{i}{\varepsilon}h\left(\frac{\partial h}{\partial X}\right)\left(\frac{\partial^2\Theta}{\partial T^2}Ae^{i\frac{\Theta(X,T)}{\varepsilon}}+\frac{i}{\varepsilon}\left(\frac{\partial\Theta}{\partial T}\right)^2\frac{\partial\Theta}{\partial T}Ae^{i\frac{\Theta(X,T)}{\varepsilon}}\right)\right]=$$
$$\frac{i}{\varepsilon}\left(\frac{\partial h}{\partial X}\right)^2\frac{\partial^2\Theta}{\partial T^2}Ae^{i\frac{\Theta(X,T)}{\varepsilon}}-\frac{1}{\varepsilon^2}\left(\frac{\partial h}{\partial X}\right)^2\left(\frac{\partial\Theta}{\partial T}\right)^2\frac{\partial\Theta}{\partial T}Ae^{i\frac{\Theta(X,T)}{\varepsilon}} \tag{B12}$$

Thus, we arrive

$$\frac{\varepsilon^2}{3}\frac{\partial^2}{\partial X\partial T}\left[h\left(\frac{\partial h}{\partial X}\right)\left(\frac{\partial\eta}{\partial T}\right)\right]=\frac{\varepsilon^2}{3}\left(\frac{\partial h}{\partial X}\right)^2\frac{\partial^2 A}{\partial T^2}e^{i\frac{\Theta(X,T)}{\varepsilon}}+\frac{\varepsilon^2}{3}h\left(\frac{\partial h}{\partial X}\right)\frac{\partial^3 A}{\partial X\partial T^2}e^{i\frac{\Theta(X,T)}{\varepsilon}}$$
$$+\frac{i\varepsilon}{3}h\left(\frac{\partial h}{\partial X}\right)\frac{\partial^2 A}{\partial T^2}\frac{\partial\Theta}{\partial X}e^{i\frac{\Theta(X,T)}{\varepsilon}}+\frac{i\varepsilon}{3}\left(\frac{\partial h}{\partial X}\right)^2\frac{\partial^2\Theta}{\partial T^2}Ae^{i\frac{\Theta(X,T)}{\varepsilon}}-\frac{i}{3}\left(\frac{\partial h}{\partial X}\right)^2\left(\frac{\partial\Theta}{\partial T}\right)^2\frac{\partial\Theta}{\partial T}Ae^{i\frac{\Theta(X,T)}{\varepsilon}} \tag{B13}$$

Finally, the wave equation becomes,

$$\varepsilon^2\frac{\partial^2 A}{\partial T^2}e^{i\frac{\Theta(X,T)}{\varepsilon}}+i\varepsilon\frac{\partial\Theta}{\partial T}\frac{\partial A}{\partial X}e^{i\frac{\Theta(X,T)}{\varepsilon}}+i\varepsilon\frac{\partial^2\Theta}{\partial T^2}Ae^{i\frac{\Theta(X,T)}{\varepsilon}}+i\varepsilon\frac{\partial\Theta}{\partial T}\frac{\partial A}{\partial T}e^{i\frac{\Theta(X,T)}{\varepsilon}}-\left(\frac{\partial\Theta}{\partial T}\right)^2Ae^{i\frac{\Theta(X,T)}{\varepsilon}}$$
$$-\varepsilon^2\left[g\frac{\partial h}{\partial X}\frac{\partial A}{\partial X}e^{i\frac{\Theta(X,T)}{\varepsilon}}+gh\frac{\partial^2 A}{\partial X^2}e^{i\frac{\Theta(X,T)}{\varepsilon}}\right]-\frac{\varepsilon^4}{3}\left(\frac{\partial h}{\partial X}\right)^2\frac{\partial^2 A}{\partial T^2}e^{i\frac{\Theta(X,T)}{\varepsilon}}-\frac{\varepsilon^4}{3}h\left(\frac{\partial h}{\partial X}\right)\frac{\partial^3 A}{\partial X\partial T^2}e^{i\frac{\Theta(X,T)}{\varepsilon}}$$
$$-\frac{i\varepsilon^3}{3}h\left(\frac{\partial h}{\partial X}\right)\frac{\partial^2 A}{\partial T^2}\frac{\partial\Theta}{\partial X}e^{i\frac{\Theta(X,T)}{\varepsilon}}-\frac{i\varepsilon^3}{3}\left(\frac{\partial h}{\partial X}\right)^2\frac{\partial^2\Theta}{\partial T^2}Ae^{i\frac{\Theta(X,T)}{\varepsilon}}-\frac{i\varepsilon^2}{3}\left(\frac{\partial h}{\partial X}\right)^2\left(\frac{\partial\Theta}{\partial T}\right)^2\frac{\partial\Theta}{\partial T}Ae^{i\frac{\Theta(X,T)}{\varepsilon}}=0 \tag{B14}$$

We consier until the second order,

ε^0-order:

$$\left(\frac{\partial\Theta}{\partial T}\right)^2A=0 \tag{B15}$$

ε-order:

$$\frac{\partial\Theta}{\partial T}\frac{\partial A}{\partial X}+\frac{\partial^2\Theta}{\partial T^2}A+\frac{\partial\Theta}{\partial T}\frac{\partial A}{\partial T}=0 \tag{B16}$$

ε^2-order:

$$\frac{\partial^2 A}{\partial T^2} - g\frac{\partial h}{\partial X}\frac{\partial A}{\partial X} - gh\frac{\partial^2 A}{\partial X^2} - \frac{i}{3}\left(\frac{\partial h}{\partial X}\right)^2\left(\frac{\partial \Theta}{\partial T}\right)^2\frac{\partial \Theta}{\partial T}A = 0 \tag{B17}$$

Thus, we have equation for the amplitude (B17 and B15),

$$\frac{\partial^2 A}{\partial T^2} - g\frac{\partial h}{\partial X}\frac{\partial A}{\partial X} - gh\frac{\partial^2 A}{\partial X^2} = 0 \tag{B18}$$

And for the phase

$$A\frac{\partial^2 \Theta}{\partial T^2} + \left(\frac{\partial A}{\partial X} + \frac{\partial A}{\partial T}\right)\frac{\partial \Theta}{\partial T} = 0. \tag{B19}$$

References

[1] Kharif,C., Pelinovsky,E., Slunyaev,A. Roque Waves in the Ocean, 2009, Springer Berlin, Heidelberg, https://doi.og/10/1007/978-3-540-88419-4.

[2] Pelinovsky,E., Kharif,C., Extreme Ocean Waves, (2016), Springer, Berlin.

[3] Knobler, S., Malila, M.P., Tayfun, M.A. et al. Effects of bound-wave asymmetry on North Sea rogue waves. Sci Rep 15, 20609 (2025). https://doi.org/10.1038/s41598-025-07156-6

[4] Azevedo, L., Marcon, G., Labourdette, E. et al. Comparison of sea conditions from reported rogue wave accidents based on reanalysis and hindcast datasets. Ocean Dynamics 75, 52 (2025). https://doi.org/10.1007/s10236-025-01697-0.

[5] Ning, D., Du, J., Bai, W. et al. Numerical modelling of nonlinear extreme waves in presence of wind. Acta Oceanol. Sin. 37, 90–98 (2018). https://doi.org/10.1007/s13131-018-1268-3.

[6] Wang, J., Yan, S. & Ma, Q. (2018). Deterministic numerical modelling of three-dimensional rogue waves on large scale with presence of wind. Procedia IUTAM, 26, pp. 214-226. doi: 10.1016/j.piutam.2018.03.021.

[7] Gemmrich, J., Cicon, L. Generation mechanism and prediction of an observed extreme rogue wave. Sci Rep 12, 1718 (2022). https://doi.org/10.1038/s41598-022-05671-4.

[8] Jiang, X., Zhang, T., Gao, D., and Wang, D.: Numerical investigation on spectral geometries and their relation to non-Gaussianity in sea states with occurrence of rogue waves: wind-sea dominated events, Nat. Hazards Earth Syst. Sci. Discuss. [preprint], https://doi.org/10.5194/nhess-2020-342, 2020.

[9] Kharif, C., & Pelinovsky, E. (2003). Physical mechanisms of the rogue wave phenomenon. European Journal of Mechanics - B/Fluids, 22 (6), 603–634. doi:10.1016/j.euromechflu.2003.09.002.

[10] Wagner GL, Pizzo N, Lenain L, Veron F. Transition to turbulence in wind-drift layers. Journal of Fluid Mechanics. 2023;976:A8. doi:10.1017/jfm.2023.920.

[11] Onorato,M and Proment,D., Approximate rogue wave solutions of the forced and damped nonlinear Schrödinger equation for water waves., Physics Letters A 376 (2012) 3057–3059.

[12] Gaxiola, G.O., Biswas, A., Akhmediev breathers, Peregrine solitons and Kuznetsov-Ma solitons in optical fibers and PCF by Laplace-Adomian decomposition method, Optik, 172, (2018), 930-939. https://doi.org/10.1016/j.ijleo.2018.07.102.

[13] Peregrine, D. H. (1983). "Water waves, nonlinear Schrödinger equations and their solutions". J. Austral. Math. Soc. B. 25: 16–43. doi:10.1017/S0334270000003891.

[14] Karjanto, N., Peregrine Soliton as a Limiting Behavior of the Kuznetsov-Ma and Akhmediev Breathers., Front. Phys., Sec. Statistical and Computational Physics, 9 (2021). https://doi.org/10.3389/fphy.2021.599767.

[15] Hsiao, Ting-Yang and Alberto Maspero. “Full Benjamin-Feir instability of capillary-gravity Stokes waves in finite depth.” (2025). arXiv:2509.17534v2.

[16] Benjamin TB, Feir JE. The disintegration of wave trains on deep water Part 1. Theory. Journal of Fluid Mechanics. 1967;27(3):417-430. doi:10.1017/S002211206700045X.
[17] Wang, Xiao, Yuan-bo Gao, Ming Wu, Feng Cai, and Xiao-guang Liu. "Freak Wave Prediction Based on the Nonlinear Schrödinger Equation." Journal of Coastal Research, 2020, 310–18. https://www.jstor.org/stable/48639045.
[18] Janssen, P. A. E. M., 2003: Nonlinear Four-Wave Interactions and Freak Waves. J. Phys. Oceanogr., 33, 863–884.
[19] Berti,M., Maspero,A., Ventura,P., Full description of Benjamin-Feir instability of stokes waves in deep water Invent. math. (2022) 230:651–711.
[20] Maleewong M, Grimshaw R. Evolution of wind-induced wave groups in water of finite depth. Journal of Fluid Mechanics. 2024;985:A2. doi:10.1017/jfm.2024.237.
[21] Longuet-Higgins, M. S. (1984). Statistical Properties of Wave Groups in a Random Sea State. Philosophical Transactions of the Royal Society of London. Series A, Mathematical and Physical Sciences, 312(1521), 219–250. http://www.jstor.org/stable/37397.
[22] Kharif,C & Touboul,J., Under which conditions the Benjamin-Feir instability may spawn an extreme wave event: A fully nonlinear approach., Eur. Phys. J. Special Topics 185, 159–168 (2010).
~~[23] Yulihastin, E., Fathrio, I., Nugroho, G.A. et al. High wind associated with bow echo mesovortex over Cimenyan, Indonesia. Meteorol Atmos Phys 137, 47 (2025). https://doi.org/10.1007/s00703-025-01095-7.~~
[24] Brunetti, M., Marchiando, N., Berti,N., Kasparian, J., Nonlinear fast growth of water waves under wind forcing, Physics Letters A, 378 (2014) 1025-1030.
[25] Fedele, F., Brennan, J., Ponce de León, S. et al. Real world ocean rogue waves explained without the modulational instability. Sci Rep 6, 27715 (2016). https://doi.org/10.1038/srep27715.
[26] Azevedo, L., Marcon, G., Meyers, S., and Luther, M.: Rogue Wave Indicators from Global Models and Buoy Data, EGUsphere [preprint], https://doi.org/10.5194/egusphere-2025-2031, 2025.
[27] Maleewong M, and Grimshaw RHJ. Amplification of Wave Groups in the Forced Nonlinear Schrödinger Equation. Fluids. 7(7), (2022); 233-245. https://doi.org/10.3390/fluids7070233.
[28] Osborne, A. R. (2010). Nonlinear Ocean Waves and the Inverse Scattering Transform. Academic Press.